An Investigation of Delayless Subband Adaptive Filtering for Multi-Input Multi-Output Active Noise Control Applications

Jordan Cheer and Stephen Daley

Abstract

The broadband control of noise and vibration using multi-input, multi-output (MIMO) active control systems has a potentially wide variety of applications. However, the performance of MIMO systems is often limited in practice by high computational demand and slow convergence speeds. In the somewhat simpler context of single-input, single-output broadband control, these problems have been overcome through a variety of methods including subband adaptive filtering. This paper presents an extension of the subband adaptive filtering technique to the MIMO active control problem and presents a comprehensive study of both the computational requirements and control performance. The implementation of the MIMO filtered-x LMS algorithm using subband adaptive filtering is described and the details of two specific implementations are presented. The computational demands of the two MIMO subband active control algorithms are then compared to that of the standard full-band algorithm. This comparison shows that as the number of subbands employed in the subband algorithms is increased, the computational demand is significantly reduced compared to the full-band implementation provided that a restructured analysis filter-bank is employed. An analysis of the convergence of the MIMO subband adaptive algorithm is then presented and this demonstrates that although the convergence of the control filter coefficients is dependent on the eigenvalue spread of the subband Hessian matrix, which reduces as the number of subbands is increased, the convergence of the cost function is limited for large numbers of subbands due to the simultaneous increase in the weight stacking distortion. The performance of the two MIMO subband algorithms and the standard full-band algorithm has then been assessed through a series of time-domain simulations of a practical active control system and it has been shown that the subband algorithms are able to achieve a significant increase in the convergence speed compared to the full-band implementation.

Index Terms

Active noise control, Active vibration control, Delayless subband adaptive filtering, MIMO

J. Cheer is with the Institute of Sound and Vibration Research, University of Southampton, Southampton, Hampshire, SO17 1BJ, U.K. (e-mail: j.cheer@soton.ac.uk).

S. Daley is with the Institute of Sound and Vibration Research, University of Southampton, Southampton, Hampshire, SO17 1BJ, U.K. (e-mail: s.daley@soton.ac.uk).

I. INTRODUCTION

For many large scale and dynamically complex systems, the active control of broadband noise and vibration presents a challenging problem due to both the computational demand and the slow convergence speed [1], [2]. In order to reduce both the computational demand and the convergence time compared to the widely employed filtered-reference least mean square (filtered-x LMS) algorithm, a number of alternative control algorithms have been proposed as summarised in [1], [2], [3]. For example, a reduction in the computational demand compared to the filtered-x LMS algorithm has been achieved by both the filtered-error, or adjoint algorithm [4] and the Douglas algorithm [5]. However, these algorithms do not improve the speed of convergence. This, however, can most straightforwardly be achieved using a variable step-size LMS algorithm [6], [7]. More significant increases in the convergence speed can be obtained by employing alternative algorithms such as the recursive least squares (RLS) algorithm [8], which increases the convergence speed at the expense of increased computational demand. Improvements in the convergence speed without the computational demands of the RLS algorithm have been achieved using hybrid algorithms that combine the LMS and RLS adaptation methods [9], as well as through the use of affine projection based algorithms [10]. The computational problem associated with large-scale active noise control systems has also recently been addressed by exploiting the parallel processing provided by graphics processing units [11].

An alternative approach to potentially improving both the convergence speed and computational efficiency of active noise control systems is to employ a frequency domain processing strategy [12], [13], [14]. In general, these methods achieve a reduction in the computational demand by converting the time domain convolution into a frequency domain multiplication, and under certain conditions can allow frequency dependent convergence gains [12]. Due to the block-based processing of frequency domain adaptive algorithms, a delay is introduced into the update of the control filter coefficients [13] and this can limit performance. An alternative method of implementing the adaptive control algorithm in frequency bands was proposed by Morgan and Thi [15] and is referred to as the delayless subband adaptive filtering architecture. This method avoids the block delay inherent in frequency domain algorithms by performing the subband signal processing in the time domain.

The delayless subband adaptive filtering method involves decomposition of the broadband error and reference signals into a number of subbands; decimation of the subband signals; adaptation of the subband control filter weights; stacking of the subband control filter weights in the frequency domain to form the fullband control filter; inverse Fourier transformation of the fullband control filter response; and the implementation of the fullband control filter in the time domain. In the context of active noise and vibration control, the delayless subband adaptive filtering method has generally been investigated in the context of single-input, single-output (SISO) systems [15], [16], [17], [18]. Although in this case it has been shown that significant improvements in the convergence speed and reductions in the computational demand can be achieved, it has been acknowledged that the potential gains of employing a subband method are even greater for multi-input, multi-output (MIMO) systems and the increase in convergence speed has been investigated, for example, for the related application of room response equalisation [19].

In the context of MIMO broadband active noise control systems, there has been limited work on the implementation and investigation of the delayless subband adaptive filtering method, perhaps due to the increased complexity compared to the equalisation problem. A discussion of the factors concerning the implementation of a multichannel delayless subband active noise control system has been presented in [2], [20], and in particular it has been shown that the computational saving is significantly greater than for the SISO case. However, despite the computational saving and the assumed increase in convergence speed, the potential improvements in performance achieved by the delayless subband architecture have not been investigated in the context of a MIMO active control system. Therefore, this paper investigates the performance of the MIMO subband active noise control system and presents a comprehensive study into how the computational requirements, the control performance and the convergence speed are affected by the number of subbands.

The MIMO filtered reference, or filtered-x LMS algorithm that is most commonly used in active noise control applications is first detailed in Section II and the limitations of this algorithm in terms of both convergence speed and computational demand are highlighted. In view of this, Section III-A introduces the method of implementing delayless subband adaptive filtering within the MIMO filtered-x LMS algorithm and presents two alternative implementations. Section III-B provides an analysis of the computational complexity of the considered subband implementations and in Section III-C a theoretical analysis of the convergence of the MIMO subband filtered-x LMS algorithm is presented. In Section IV a comprehensive investigation into how the computational complexity, convergence speed and control performance are affected by the number of subbands employed in the MIMO subband algorithms is presented for a practical active control system and comparisons are also made to the standard full-band implementation. Finally, conclusions are drawn in Section V

II. MIMO FILTERED-x LMS

The MIMO filtered-x LMS algorithm has been widely employed in the context of active noise and vibration control and was originally proposed as an extension to the SISO filtered-x LMS algorithm in the late 1980s [21]. The MIMO filtered-x LMS algorithm is shown in Figure 1. This system attempts to minimise the L_e error signals, $\mathbf{e}$, by driving the M control sources with the L_x reference signals, $\mathbf{x}$, via the bank of ML_x control filters, $\mathbf{W}$. The primary path between the noise source and the error sensors is characterised by the response, $\mathbf{P}(z)$ and the plant, or secondary path is characterised by the response $\mathbf{G}(z)$. If it is assumed that the control filters are time-invariant, then the vector of error signals can be approximated as [1], [21]

$$\mathbf{e}(n) = \mathbf{d}(n) + \mathbf{R}(n)\mathbf{w}(n) \tag{1}$$

where $\mathbf{d}(n)$ is the vector of L_e disturbance signals, $\mathbf{R}(n)$ is the $L_e \times ML_xI$ matrix of filtered reference signals and $\mathbf{w}(n)$ is the vector of ML_xI filter coefficients of the I-th order control filters. The disturbance signals are generated by filtering the reference signals, $\mathbf{x}$, by the primary path response, $\mathbf{P}(z)$, as shown in Figure 1. The matrix of filtered reference signals is formulated from the L_x reference signals filtered by the model of the plant

response given by $\hat{\mathbf{G}}$; that is,

$$\mathbf{R}(n) = \begin{bmatrix} \mathbf{r}_1^T(n) & \mathbf{r}_1^T(n-1) & \cdots & \mathbf{r}_1^T(n-I+1) \\ \mathbf{r}_2^T(n) & \mathbf{r}_2^T(n-1) & & \\ \vdots & & & \\ \mathbf{r}_{L_e}^T(n) & \mathbf{r}_{L_e}^T(n-1) & \cdots & \mathbf{r}_{L_e}^T(n-I+1) \end{bmatrix} \tag{2}$$

where

$$\mathbf{r}_{l_e}(n) = \begin{bmatrix} r_{l_e 11}(n) & r_{l_e 12}(n) & \cdots \\ & r_{l_e 1 L_x}(n) & r_{l_e 21}(n) & \cdots & r_{l_e M l_x}(n) \end{bmatrix}^T \tag{3}$$

and

$$r_{l_e m l_x} = \hat{\mathbf{g}}_{l_e m}^T \mathbf{x}_{l_x}, \tag{4}$$

where $\hat{\mathbf{g}}_{l_e m}$ is the vector of J filter coefficients of the finite impulse response (FIR) filter which models the plant response between the l_e-th error sensor and the m-th control source, and $\mathbf{x}_{l_x}$ is the vector of the l_x-th reference signal over the previous J sample periods. The ML_xI vector of control filter coefficients in (1) is constructed as

$$\mathbf{w} = \begin{bmatrix} \mathbf{w}_1^T & \mathbf{w}_2^T & \cdots & \mathbf{w}_{I-1}^T \end{bmatrix} \tag{5}$$

where $\mathbf{w}_i$ is the ML_x vector of coefficients given by

$$\mathbf{w}_i = \begin{bmatrix} w_{11i}^T & w_{12i}^T & \cdots & w_{1L_x i}^T & w_{21i}^T & \cdots & w_{ML_x i}^T \end{bmatrix}. \tag{6}$$

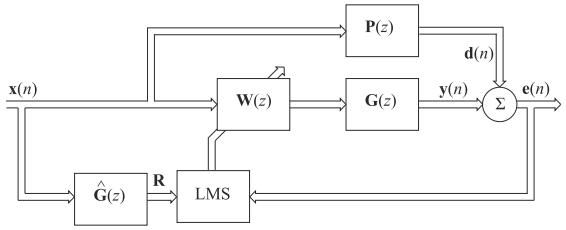

Fig. 1: MIMO filtered-x LMS active control system.

In multichannel active control applications, the controller is generally adapted to minimise the cost function given by the sum of the squared error signals. Using (1) this cost function can be written as

$$C = \mathbf{e}^T(n)\mathbf{e}(n) \tag{7}$$

$$= \mathbf{w}^T(n)\mathbf{R}^T(n)\mathbf{R}(n)\mathbf{w}(n) + \cdots$$

$$2\mathbf{w}^T(n)\mathbf{R}^T(n)\mathbf{d}(n) + \mathbf{d}^T(n)\mathbf{d}(n). \tag{8}$$

Using the method of steepest-descent, this cost function can be minimised by adapting the vector of filter coefficients according to the update equation

$$\mathbf{w}(n+1) = \mathbf{w}(n) - \alpha \mathbf{R}^T(n)\mathbf{e}(n), \tag{9}$$

where α is the convergence gain and this algorithm is generally referred to as the filtered-x LMS algorithm.

A. Convergence and Stability

A relatively straightforward analysis of the convergence of the multichannel filtered-x LMS algorithm can be performed by assuming that the control filter coefficients are changing slowly compared with the dynamic response of the plant. Although this assumption is generally not true in a practical implementation, it has been shown to provide a good indication of the algorithm's performance [22]. The convergence behaviour of the multichannel filtered-x LMS algorithm can be analysed by first substituting (1) into (9) and using the estimated matrix of filtered reference signals, $\widehat{\mathbf{R}}^T(n)$, in the update equation, which gives

$$\mathbf{w}(n+1) = \mathbf{w}(n) - \alpha \left[\widehat{\mathbf{R}}^T(n)\mathbf{d}(n) + \widehat{\mathbf{R}}^T(n)\mathbf{R}(n)\mathbf{w}(n)\right]. \tag{10}$$

Assuming that the algorithm is stable, then it can be seen from (10) that the vector of filter coefficients will have converged to its steady-state value when the expectation of the term in square brackets is equal to zero. The steady-state vector of control filter coefficients is thus given by

$$\mathbf{w}_\infty = -\left\{E\left[\widehat{\mathbf{R}}^T(n)\mathbf{R}(n)\right]\right\}^{-1} E\left[\widehat{\mathbf{R}}^T(n)\mathbf{d}(n)\right]. \tag{11}$$

Assuming that the filter coefficients are statistically independent from the reference signals [1], the expectation behaviour of the filter coefficient update equation given by (10) can then be expressed as

$$\begin{aligned} E\left[\mathbf{w}(n+1) - \mathbf{w}_\infty\right] &= \cdots \\ &\left[\mathbf{I} - \alpha E\left[\widehat{\mathbf{R}}^T(n)\mathbf{R}(n)\right]\right] E\left[\mathbf{w}(n) - \mathbf{w}_\infty\right]. \end{aligned} \tag{12}$$

It can be seen from (12) that the algorithm will reach the steady-state solution if the term in square brackets is less than unity and, therefore, the algorithm will converge provided that

$$0 < \alpha < \frac{2\Re(\lambda_{max})}{|\lambda_{max}|^2}, \tag{13}$$

where λ_{max} is the largest eigenvalue of the Hessian matrix, $E\left[\widehat{\mathbf{R}}^T(n)\mathbf{R}(n)\right]$. The convergence behaviour of the filtered-x LMS algorithm can then be analysed by expressing the Hessian matrix in terms of the matrix of its eigenvectors, $\mathbf{Q}$, and the diagonal matrix of its eigenvalues, $\mathbf{\Lambda}$, as

$$E\left[\widehat{\mathbf{R}}^T(n)\mathbf{R}(n)\right] = \mathbf{Q}\mathbf{\Lambda}\mathbf{Q}^{-1}. \tag{14}$$

Substituting this expansion into (12) and multiplying through by the inverse of the matrix of eigenvectors then gives the simplified expression

$$\mathbf{v}(n+1) = \left[\mathbf{I} - \alpha\mathbf{\Lambda}\right]\mathbf{Q}^{-1}\mathbf{v}(n), \tag{15}$$

where $\mathbf{v}(n)$ is the vector of transformed normalised averaged filter coefficients given by $\mathbf{Q}^{-1}E\left[\mathbf{w}(n+1)-\mathbf{w}_{\infty}\right]$. From (15) it can be seen that, since $\mathbf{\Lambda}$ is a diagonal matrix, the multichannel filtered-x LMS algorithm converges in a series of independent *modes*. If the algorithm is stable then the time constants of these independent modes are determined by the magnitudes of the real parts of the eigenvalues of the Hessian matrix, such that the mode corresponding to the largest eigenvalue converges with the shortest time constant, while the mode corresponding to the minimum eigenvalue converges with the longest time constant [1], [23], [22]. The eigenvalue spread, or the ratio of the largest to the smallest eigenvalues, therefore describes the limits on the convergence of the multichannel filtered-x LMS algorithm. The eigenvalue spread in the case of this broadband multichannel control problem is determined by the spectral range of the reference signals; the correlation between the reference signals; and the dynamics of the plant response between the actuators and sensors [1]. In general, the combination of these effects can lead to a very large eigenvalue spread and, therefore, very slow convergence.

B. Computational Complexity

In addition to the slow convergence of the broadband multichannel control algorithm, since long FIR filters are generally required for both the plant response modelling and the control filters, the computational demand quickly becomes very large. The main contributions to the computational demand of the broadband MIMO filtered-x LMS active control system shown in Figure 1 are the generation of the filtered reference signals, the adaptation of the control filters and the generation of the control signals; the multiplications required for each of these processes are summarised in Table I. In most active noise and vibration control applications, the impulse responses required to model the plant response and to achieve broadband control are rather long [15]. This means that, since the number of multiplications required by the broadband filtered-x LMS algorithm is a function of the number of filter coefficients in the control filter and the plant model filter, the computational demand of a broadband active controller quickly becomes very large.

TABLE I: The number of multiplications per sample for the MIMO full-band filtered-x LMS active control system

Operation	Multiplications
Filtered-x generation	ML_xL_eJ
Control filters update	$ML_x(L_e+1)I$
Control signals generation	ML_xI
Total	$ML_xL_e(J+I)+2ML_xI$

III. MIMO DELAYLESS SUBBAND FILTERED-x LMS

In order to reduce the computational requirements and increase the convergence speed of the MIMO filtered-x LMS algorithm it has been proposed that delayless subband adaptive filtering methods could be employed. The delayless subband adaptive filtering method was originally proposed in [15] for the SISO system and its application

to MIMO systems has been previously suggested [20]. However, although the computational requirements of the MIMO subband filtered-x LMS algorithm have been considered [20], [2], as highlighted in the introduction, the assumed increase in convergence speed has not been formally investigated and the influence of the number of subbands on the control performance has not been investigated. The implementation of the MIMO filtered-x LMS algorithm using delayless subband adaptive filtering is first described in this section; the computational requirements are then investigated in Section III-B and the convergence behaviour is investigated in Section III-C and finally the performance limitations are investigated and compared to the full-band implementation in Section IV.

A. MIMO Subband Implementation

The MIMO formulation of the original SISO delayless subband adaptive filtering architecture proposed by Morgan and Thi [15] is shown in Figure 2 for the filtered-x LMS algorithm. From this block diagram it can be seen that the control signal generation and the filtering of the reference signals by the model of the plant are still both performed as in the broadband controller shown in Figure 1, however, the filter weight adaptation is now performed in K subbands. This subband adaptation requires that the broadband filtered reference and error signals are first filtered by an analysis filter-bank, $\mathbf{h}(z)$, to generate the K subband components of these signals. The subband signals are then decimated by a factor D, which is possible due to the reduced bandwidth of the signals and provides a significant computational saving. In each of the subbands the subband filter coefficients, $\mathbf{w}_k^{SAF}$, can then be updated according to the multichannel filtered-x LMS algorithm as

$$\mathbf{w}_k^{SAF}(n+1) = \mathbf{w}_k^{SAF}(n) - \alpha_k \mathbf{R}_k^H(n)\mathbf{e}_k(n), \tag{16}$$

where $\mathbf{w}_k^{SAF}$ is the vector of ML_xI_{SAF} filter coefficients corresponding to the I_{SAF}-th order control filter for the k-th subband, α_k is the convergence gain in the k-th subband, $\mathbf{R}_k$ is the $L_e \times ML_xI_{SAF}$ matrix of filtered reference signals in the k-th subband, and $\mathbf{e}_k$ is the vector of L_e error signals in the k-th subband. Each of the ML_x control filter impulse responses in each of the K subbands is then Fourier transformed and the frequency responses of these subband control filters are combined via a weight stacking method to form the responses of the broadband control filters in the frequency domain. The ML_x frequency responses of the broadband control filters are then inverse Fourier transformed to give the impulse responses of the broadband control filter, which is formed as a vector of ML_xI coefficients as described by (5) and (6).

In addition to the significant computational saving that is achieved through the subband filtering structure shown in Figure 2, a further computational saving can be achieved by implementing the reference signal filtering in each of the subbands, as shown in Figure 3. This alteration to the original delayless subband algorithm was proposed by Park *et al* for a SISO system[16], and means that the plant model filtering is implemented at the decimated sampling rate and that the subband-decomposed plant response models can be implemented with significantly shorter impulse responses. In [16] the reduction in computational complexity achieved by this restructuring of the filtered-x subband architecture is considered in the context of a SISO system, however, the computational saving will be investigated in Section III-B for a multichannel active control system.

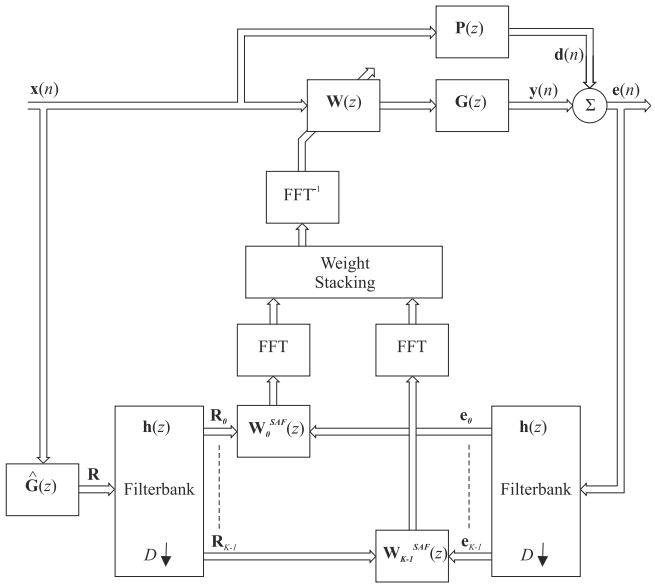

Fig. 2: MIMO filtered-x LMS delayless subband active control system.

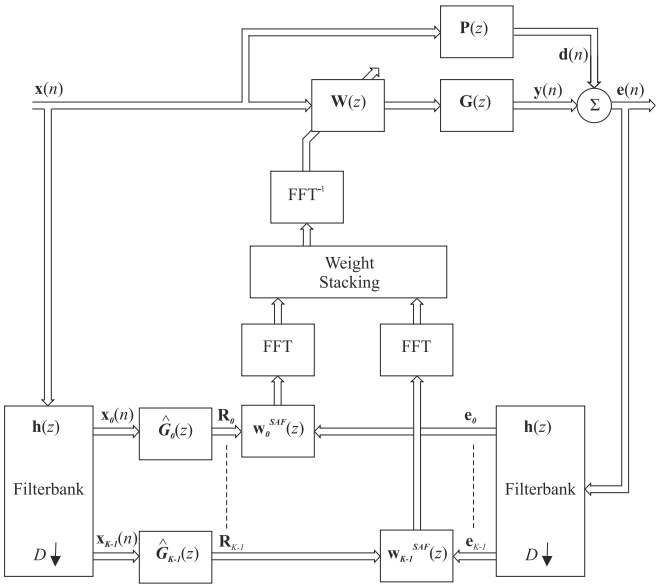

Fig. 3: MIMO filtered-x LMS delayless subband active control system with subband plant modelling.

1) Analysis Filter-bank and Decimation: As shown in both Figures 2 and 3, the implementation of the subband active control system requires an analysis filter-bank, signal decimation and complimentary weighting stacking process. There are a number of different methods of implementing these components of the subband adaptive filtering systems and these different methods have been discussed in the context of both active control [15], [16], [17] and more generally for adaptive signal processing [24], [25], [26], [27]. In general the different methods provide a trade-off between computational complexity, spectral leakage, delay and aliasing effects. In the context of active noise control, Morgan and Thi [15] propose the use of a polyphase FFT technique to implement the analysis filter-bank, in which a prototype linear-phase FIR filter is designed and modulated to produce the filter-bank. However, since this prototype filter is designed to reduce the spectral leakage between the subbands, a high-order filter is required and this introduces a significant delay into the system. Milani *et al* [17] show that this additional delay has a higher impact on the performance of the subband active control system than the spectral leakage and they propose an alternative method employing a simple Uniform Discrete Fourier Transform Modulated (UDFTM) filter-bank and complementary weight stacking method [17]. In the case of the SISO system this method has been shown to allow a higher number of subbands compared to the method of Morgan and Thi [15] and therefore reduces the computational demand whilst achieving comparable levels of control [17].

The UDFTM filter-bank employed in [17] consists of K subband filters, where the transfer function of the k-th filter is given by

$$H_k(z) = H_0(ze^{-j2\pi k/K}), \tag{17}$$

where H_0 is the prototype low-pass FIR filter with K coefficients given by

$$H_0(z) = 1 + z^{-1} + \cdots + z^{-K+1}. \tag{18}$$

The full bank of K filters is then constructed as

$$\mathbf{h}(z) = \begin{bmatrix} H_0(z) & H_1(z) & \cdots & H_{K-1}(z) \end{bmatrix}. \tag{19}$$

The UDFTM filter-bank is the simplest FIR perfect reconstruction filter-bank [24] and the transfer functions of the full bank of K filters, $\mathbf{h}(z)$, can in fact be expressed in terms of the K-th order discrete Fourier transform (DFT) matrix, $\mathbf{F}$, as

$$\mathbf{h}(z) = \frac{1}{K}\mathbf{F}^* \begin{bmatrix} 1 \\ z^{-1} \\ \vdots \\ z^{-K+1} \end{bmatrix}, \tag{20}$$

where * denotes the complex conjugate operator and is present due to the definition of the DFT matrix [24]. In practice, this filter-bank can be implemented using a tapped delay line with K taps followed by an inverse Fourier transform [17] and is, therefore, relatively straightforward to implement.

As shown in Figures 2 and 3, the subband signals output from the analysis filter-bank are decimated by a factor of D. The appropriate choice of decimation factor is dependent on the level of attenuation provided by the side-lobes

of the subband analysis filters, since the resulting out-of-band signals will cause aliasing through the decimation process. The UDFTM filter-bank has a lower level of sideband attenuation than provided by the analysis filter-bank employed by Morgan and Thi [15] and, therefore, in order to limit the effects of aliasing Milani *et al* [17] propose a decimation factor of $D = \frac{K}{4}$, which is half of that employed in [15]. This means that the computational demand of the method proposed by Milani *et al*, and outlined here, has a slightly higher computational demand than the original method proposed in [15] when the same number of subbands is used in both methods. However, it is possible to implement the method proposed by Milani *et al* with a significantly higher number of subbands than the original Morgan and Thi method, which provides a significant computational saving and ultimately means that this method can outperform the original method.

The block diagram showing the practical implementation of the analysis filter-bank and decimation process proposed by Milani *et al* [17] for a single input channel is shown in Figure 4a. From this block diagram it can be seen that the input signal is passed through a tapped delay line of length K. This $K \times 1$ vector of delayed input signals is then inverse Fourier transformed and then decimated by the decimation factor, D. This means that the output of the IFFT block is actually only used once every D samples and this leads to a large computational overhead. This, however, can be significantly reduced by restructuring the analysis filter-bank and decimation process using the Noble identity [24] and this leads to the equivalent implementation shown in Figure 4b. In this case the IFFT is computed at the decimated sample rate and the computational demand is thus reduced by the decimation factor. It should be highlighted that the Noble identity is not an approximation and, therefore, although the decimation now occurs before the IFFT, this restructuring does not introduce additional aliasing. That is, because the tapped delay is longer than the number of samples removed by the decimation factor, no information is lost by interchanging the two blocks. The Noble identity is not employed in [17], but it facilitates a significant reduction in the computational demand, particularly when implementing a multichannel adaptive control system in which an analysis filter-bank is required for at least each error signal and each reference signal.

(a) Standard implementation.

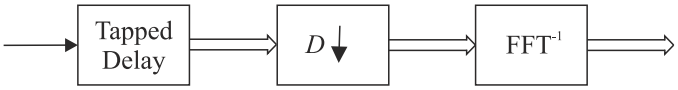

(b) Alternative implementation using the Noble identity.

Fig. 4: Block diagrams of two alternative implementations of the UDFTM analysis filter-bank and signal decimation.

2) Weight Stacking Method: In order to form the full-band control filters, $\mathbf{w}$, from the K subband control filters, $\mathbf{w}_k^{SAF}$, it is necessary to employ a synthesis filter-bank, or weight stacking procedure, that is complementary to the

analysis filter-bank [24], [25]. As such, a variety of different synthesis filter-banks have been proposed, however, the method put forward in [17] will be outlined here since it is complementary to the analysis filter-bank described in the previous section.

It is first important to highlight that the subband signals output from the analysis filter-bank described in the previous section are complex and, therefore, the subband filter adaptation described by (16) is a complex LMS algorithm. However, since the full-band signals are real-valued and the analysis filter-bank response is complex conjugate symmetric, only the first $K/2+1$ subbands need to be processed [15], [17], [25]. The first stage in the weight stacking procedure is to calculate the $2I_{SAF}$ point FFT of each of the subband filters by using zero padding to give the Discrete Fourier Transform (DFT) coefficients for each of the subbands. This process produces the $ML_x \times 2I_{SAF}$ matrix $\mathbf{W}_k^{SAF}$, which contains the $2I_{SAF}$ DFT coefficients for each of the ML_x channels in the multichannel control system. The full-band control filter matrix of DFT coefficients, $\mathbf{W}$, is then constructed from these subband DFT coefficients. Specifically, the $ML_x \times 2I$ matrix of full-band coefficients can be constructed by extending the single channel formulation presented by Milani *et al* [17] to give

$$\begin{aligned} W_{ml_x}[i] &= W_{ml_x}^{SAF}{}_{\left(\left(\lfloor \frac{iK}{2I} \rfloor\right)\right)_K}\left[\left((i)\right)_{\frac{8I}{K}}\right] && \text{for} \quad i \in [0, I], \\ W_{ml_x}[i] &= W_{ml_x}^{*}[2I - i] && \text{for} \quad i \in [I, 2I] \end{aligned} \tag{21}$$

where $W_{ml_x}[i]$ is the i-th DFT bin of the full-band control filter corresponding to the m-th control source and the l_x-th reference signal, $\left(\left(\lfloor \frac{iK}{2I} \rfloor\right)\right)_K$ determines which subband the DFT coefficient should be taken from, and $\left[\left((i)\right)_{\frac{8I}{K}}\right]$ determines the index of the subband DFT coefficient. $((\cdots))_K$ indicates the modulo-K operation and $\lfloor \cdots \rfloor$ indicates the floor operation. The second line in (21) indicates that the second half of the full-band control filter responses is formed in complex conjugate symmetry to the first half of their responses. This weight stacking method requires that the number of filter coefficients in each of the subband adaptive filters, I_{SAF}, should be greater than or equal to $4I/K$. Finally, as shown in Figures 2 and 3 the full-band filter coefficients are obtained by taking the inverse FFT of the weight stacked full-band DFT responses, $\mathbf{W}$. These filter coefficients are then structured as the vector of ML_xI coefficients as described by (5) and (6).

B. MIMO Subband Computational Complexity

One of the main motivations for the subband adaptive processing method is the potentially significant computational saving and this may be particularly significant for the multichannel implementation. This has been discussed in [2], [20] for the MIMO control system with a single [20] and multiple [2] reference signals, however, a comparison between the standard full-band method and the specific subband implementations described in Section III will be compared here in terms of the number of multiplications required per sample. In particular, the difference in the computational requirements for the two multichannel subband active noise control architectures shown in Figures 2 and 3 will be compared and the significance of employing the Noble identity to restructure the analysis filter bank implementation on the overall computational demand will be demonstrated. Furthermore, a clear graphical comparison of the full-band and subband algorithms will be presented, which will provide insight into the trade-off

between the computational demand and the performance, which has not previously been investigated for the MIMO system.

1) Reference signal filtering: The generation of the filtered reference signals is central to the implementation of the filtered-x LMS algorithm. For the standard subband architecture proposed in [15] and shown in Figure 2, the matrix of filtered reference signals, $\mathbf{R}$, is generated at the full sample rate, Fs, by filtering the L_x reference signals using the ML_e models of the plant response, $\hat{\mathbf{G}}$. If the MIMO model of the plant response is implemented using a bank of FIR filters of length J, as described in Section II, then the number of multiplications per sample is

$$c_1 = ML_eL_xJ. \tag{22}$$

It is typical that the length for the plant modelling filters, J, to be several hundred coefficients long in order to provide accurate modelling for acoustic and structural systems. Therefore, the computational demand of calculating the filtered reference signals rapidly increases as the number of channels in the control system increases.

This problem can be limited by implementing the multichannel subband control system as shown in Figure 3, where the subband reference signals are filtered by subband plant models. Although this modification requires complex filtering due to the subband reference signals being complex, it has two benefits in terms of computational complexity. Firstly, the reference signal filtering is implemented at the decimated sample rate, Fs/D, and secondly, the subband plant model filters, $\hat{\mathbf{G}}_k$, must only be accurate over the bandwidth of the corresponding subband signals. This means that the number of coefficients required for each subband plant model filter, J_{SAF}, can be reduced as the bandwidth of the subbands is reduced. The number of multiplications required per sample at the full sample rate of Fs for this implementation is then

$$c_1' = 3ML_eL_xJ_{SAF}\left(\frac{K/2+1}{D}\right), \tag{23}$$

where the factor of $(K/2+1)$ is due to the subband plant model filtering being implemented in the $K/2+1$ subbands corresponding to the real part of the frequency spectrum, the factor of 3 is due to the filtering process being complex, and the decimation factor is $D = K/4$, which gives the computational demand as

$$c_1' = 3ML_eL_xJ_{SAF}\left(2+\frac{4}{K}\right). \tag{24}$$

2) Subband filtering and decimation: The subband filtering and signal decimation process can be implemented using two different formulations, as shown in Figure 4. The analysis filter-bank and decimation process in Figure 4a requires one K-point inverse FFT per sample at the full sample rate of Fs, which corresponds to $K\log_2 K$ multiplications per sample. For the subband implementation shown in Figure 2, an analysis filter-bank and decimator are required for each of the ML_eL_x filtered reference signals and the L_e error signals and this results in a total number of multiplications per sample at the full sample rate of

$$c_{2,a} = (L_e + ML_eL_x)\,K\log_2 K. \tag{25}$$

However, by using the Noble identity to restructure the analysis filter-bank as shown in Figure 4b, a K-point inverse FFT is only required once per sample at the decimated sample rate of Fs/D. The number of multiplications per

sample for the subband implementation in Figure 2 is then reduced by a factor of D to give

$$c_{2,b} = (L_e + ML_eL_x)\,\frac{K\log_2 K}{D} \tag{26}$$

$$= (L_e + ML_eL_x)\,4\log_2 K. \tag{27}$$

For the alternative implementation of the subband active control system shown in Figure 3, due to the reordering of the plant model filtering and the analysis filter-banks, a significant reduction in the number of analysis filter-banks is achieved. In this implementation an analysis filter-bank and decimator are only required for the L_x reference signals and the L_e error signals, such that the number of multiplications per sample for the standard analysis filter-bank in Figure 4a is reduced to

$$c'_{2,a} = (L_e + L_x)\,K\log_2 K, \tag{28}$$

and for the restructured analysis filter-bank in Figure 4b is reduced to

$$c'_{2,b} = (L_e + L_x)\,4\log_2 K. \tag{29}$$

3) Subband weight adaptation: The adaptation of the $K/2+1$ complex subband control filter weights is performed according to equation (16) for both of the subband system implementations shown in Figures 2 and 3. The update equation given by equation (16) requires $L_eML_xI_{SAF}$ complex multiplications for the matrix multiplication $\mathbf{R}_k^T(n)\mathbf{e}_k(n)$, and a further ML_xI_{SAF} complex-real multiplications as the complex vector given by $\mathbf{R}_k^T(n)\mathbf{e}_k(n)$ is multiplied by the real-valued convergence gain, α_k. The multiplication of two complex numbers can be achieved using a minimum of 3 real multiplications, while the multiplication of a complex number by a scalar requires 2 real multiplications. For the $(K/2+1)$ subband update algorithms operating at the decimated sample rate, D, the total number of real multiplications is thus given by

$$c_3 = (3L_eML_xI_{SAF} + 2ML_xI_{SAF})\,\frac{K/2+1}{D}. \tag{30}$$

If the number of subband adaptive filter coefficients is set to the minimum required by the weight stacking method outlined in Section III-A2, which is $I_{SAF} = 4I/K$, then the number of multiplications per sample required by the subband weight adaptation is given by

$$c_3 = ML_x\,(3L_e + 2)\,\frac{8I}{K}\left(1 + \frac{2}{K}\right). \tag{31}$$

4) Weight stacking: The weight stacking process, which is described in Section III-A2, requires a $2I_{SAF}$-point FFT for each of the complex subband control filters and a $2I$-point inverse FFT of the weight stacked full-band control filters. Each of the $2I_{SAF}$-point complex FFT requires about $4I_{SAF}\log_2(2I_{SAF})$ real multiplications [15] and the $2I$-point inverse FFT requires $2I\log_2 2I$ real multiplications. The total number of real multiplications per sample is thus given by

$$c_4 = \frac{ML_x}{D}\left[\left(\frac{K}{2}+1\right)4I_{SAF}\log_2 2I_{SAF} + 2I\log_2 2I\right]. \tag{32}$$

If it is again assumed that $I_{SAF} = 4I/K$ and $D = K/4$ this can be simplified to give

$$c_4 = \frac{8ML_xI}{K}\left[\left(4 + \frac{8}{K}\right)\log_2\frac{8I}{K} + \log_2 2I\right]. \tag{33}$$

5) Full-band control signal generation: The final significant operation in the implementation of the subband active control systems is the generation of the output control signals. As can be seen from Figures 2 and 3 this filtering process is performed in the time-domain on the full-band reference signals, and is identical to the implementation in the full-band standard MIMO active control system shown in Figure 1. The number of multiplications required per sample is given by

$$c_5 = ML_xI. \tag{34}$$

In order to understand how the individual computational operations contribute to the overall computational requirement, compare the two alternative implementations outlined in Figures 2 and 3, and demonstrate the significant computational gain achieved by restructuring the analysis filter-bank as shown in Figure 4, an example multichannel control system will be considered in Section IV.

C. MIMO Subband Convergence Analysis

Although a primary motivation for the implementation of subband algorithms is the reduced computational complexity compared to the broadband alternative, a significant increase in convergence speed is also potentially possible [15]. It has been highlighted in the literature that this is expected to be even greater for the MIMO subband active noise control system, however, the convergence behaviour of the MIMO subband filtered-x LMS algorithm has not been analysed in the literature. Therefore, following the convergence and stability analysis presented in Section II-A, the convergence and stability of the subband filtered-x LMS algorithm will be analysed.

Firstly, by assuming, as in the full-band case, that the subband control filter coefficients are changing slowly compared with the dynamic response of the plant, the error signal in the k-th subband can be expressed as

$$\mathbf{e}_k(n) = \mathbf{d}_k(n) + \mathbf{R}_k(n)\mathbf{w}_k^{SAF}(n) \tag{35}$$

where $\mathbf{d}_k(n)$ is the disturbance signal in the k-th subband. The convergence behaviour of the multichannel subband filtered-x LMS algorithm can then be analysed by substituting (35) into (16) and using the matrix of subband filtered reference signals estimated via the plant model, $\widehat{\mathbf{R}}_k^T(n)$, which gives

$$\begin{aligned}\mathbf{w}_k^{SAF}(n+1) = &\cdots \\ &\mathbf{w}_k^{SAF}(n) - \alpha_k\left[\widehat{\mathbf{R}}_k^H(n)\mathbf{d}_k(n) + \widehat{\mathbf{R}}_k^H(n)\mathbf{R}_k(n)\mathbf{w}_k^{SAF}(n)\right].\end{aligned} \tag{36}$$

Assuming that the algorithm is stable, then it can be seen from (36) that the control coefficients corresponding to the k-th subband will have converged to their steady-state values when the expectation of the term in square brackets is zero. The steady-state vector of control filter coefficients in the k-th subband can then be written as

$$\mathbf{w}_{k,\infty}^{SAF} = -\left\{E\left[\widehat{\mathbf{R}_k}^T(n)\mathbf{R}_k(n)\right]\right\}^{-1} E\left[\widehat{\mathbf{R}}_k^T(n)\mathbf{d}_k(n)\right]. \tag{37}$$

Making the same independence assumptions that were made in the full-band case, the expectation behaviour of the subband filter coefficient update equation can then be expressed using the steady-state vector of subband control filter coefficients as

$$E\left[\mathbf{w}_k^{SAF}(n+1) - \mathbf{w}_{k,\infty}^{SAF}\right] = \cdots \\ \left[\mathbf{I} - \alpha_k E\left[\widehat{\mathbf{R}}_k^H(n)\mathbf{R}_k(n)\right]\right] E\left[\mathbf{w}_k^{SAF}(n) - \mathbf{w}_{k,\infty}^{SAF}\right]. \quad (38)$$

The Hessian matrix corresponding to the k-th subband can then be written using the eigenvalue decomposition as

$$E\left[\widehat{\mathbf{R}}_k^T(n)\mathbf{R}_k(n)\right] = \mathbf{Q}_k\mathbf{\Lambda}_k\mathbf{Q}_k^{-1}, \quad (39)$$

where $\mathbf{Q}_k$ is the matrix of eigenvectors and $\mathbf{\Lambda}_k$ is the diagonal matrix of eigenvalues, both corresponding to the k-th subband Hessian matrix. Substituting this expansion into (38) and multiplying through by $\mathbf{Q}_k^{-1}$ then gives the vector of transformed normalised averaged subband filter coefficients as

$$\mathbf{v}_k(n+1) = \left[\mathbf{I} - \alpha_k\mathbf{\Lambda}_k\right]\mathbf{v}_k(n), \quad (40)$$

where $\mathbf{v}(n) = \mathbf{Q}_k^{-1}E\left[\mathbf{w}_k^{SAF}(n+1) - \mathbf{w}_{k,\infty}^{SAF}\right]$. Since $\mathbf{\Lambda}_k$ is diagonal, it can be seen that (40) represents a series of independent equations, which are associated with the independent modes of convergence of the k-th subband adaptive algorithm.

From (40) it can also be seen that the control filter coefficients in the k-th subband adaptive algorithm will converge towards their steady-state value if the term in square brackets is less than unity and, therefore, the algorithm will be stable provided that the convergence gain in each subband can be set such that

$$0 < \alpha_k < \frac{2\Re(\lambda_{k_{max}})}{|\lambda_{k_{max}}|^2}, \quad (41)$$

where $\lambda_{k_{max}}$ is the maximum eigenvalue of the Hessian matrix in the k-th subband, $\widehat{\mathbf{R}}_k^H(n)\mathbf{R}_k(n)$. Once again, it should be highlighted that, since this is stability limit is based on the assumption that the control filter coefficients are changing slowly compared with the dynamic response of the plant, this limit can only be used as a relative guide and in practice the convergence gain is generally set below the upper limit indicated by this expression. However, the equivalent full-band stability limit has been widely shown to provide a useful guide in practice. Nevertheless, assuming that the convergence gain has been set such that the subband adaptive algorithm is stable, which also requires that the real parts of all of the eigenvalues are positive, then the subband algorithm will converge in a series of independent modes with time constants determined by the magnitude of the real part of the corresponding eigenvalue. The mode corresponding to the largest eigenvalue converges with the shortest time constant $(1/(\alpha_k|\lambda_{k_{max}}|))$ and that corresponding to the smallest eigenvalue converges with the longest time constant $(1/(\alpha_k|\lambda_{k_{min}}|))$. If the plant model is perfect and, therefore, $\widehat{\mathbf{R}}_k(n) = \mathbf{R}_k(n)$, all of the eigenvalues of the Hessian matrix will be positive real, and the slowest mode of convergence will have a time constant that is proportional to $\lambda_{k_{max}}/\lambda_{k_{min}}$, or the eigenvalue spread of the Hessian matrix.

From the above analysis it is clear that the convergence of each of the subband adaptive filters is governed by the corresponding subband Hessian matrix, $E\left[\widehat{\mathbf{R}}_k^H\mathbf{R}_k\right]$. Due to the inherently smaller bandwidth within a subband

algorithm compared to the full-band implementation, the subband Hessian matrix will generally have a lower spectral range than the full-band equivalent and, therefore, the subband control filter coefficients will converge to their steady-state values with a shorter time constant. Also, since the convergence gain in each subband, α_k, can be set independently, the speed of convergence in each band will only be limited by its own eigenvalue spread. However, due to the weight stacking processing required to translate the subband control filter coefficients into the full-band control filter coefficients, it is not completely clear from this analysis how any distortion introduced by the weight stacking process [18] will affect the performance and convergence in terms of the sum of the squared errors cost function. Therefore, the effect of the number of subbands on the eigenvalue spread, the control performance and convergence speed will be investigated in the following section for a practical control problem.

IV. Performance Investigation

In order to provide a comparison between the performance of the multichannel filtered-x LMS algorithm, shown in Figure 1, and the two multichannel subband algorithms, shown in Figures 2 and 3, the practical control system in Figure 5 will be investigated. This system represents the structural problem of controlling the transmission of vibration through a beam-like structure into a wall or plate. The primary disturbance in the experimental setup is provided by an inertial actuator mounted on the beam and the single reference signal is obtained from the signal driving this actuator. In the following investigation the primary actuator is driven by broadband stationary white noise; this presents a challenging test case for active noise control systems due to the unpredictability of the white noise signal. If the signal was coloured then its predicability would increase and the level of control performance would increase accordingly. The control system consists of three tri-axial accelerometer error sensors and five inertial actuator control sources, which are shown by the small cubes and cylinders in Figure 5 respectively. The five control actuators are arranged to allow control of five degrees of freedom of the plate. The MIMO control system thus consists of $M = 5$ control sources, $L_e = 9$ error sensors and $L_x = 1$ reference sensor. In the following sections, the performance of the different MIMO algorithms has been calculated via offline predications using the measured responses. This allows a significant number of system configurations to be considered and, therefore, facilitates an understanding of the performance limitations of the two subband algorithms compared to the standard fullband controller. It is worth highlighting that, as already indicated by the description of the subband algorithms in Section III, in a practical implementation the subband algorithms require multi-rate processing which can generally be implemented on standard signal processing boards.

Figure 6 shows two examples of the frequency response of the structure shown in Figure 5. Figure 6a shows the frequency response between the primary source and one error sensor and Figure 6b shows the response between one control actuator and the same error sensor. From these plots it can be seen that the system is characterised by a large number of lightly damped resonances and, therefore, presents a significant challenge to typical multichannel broadband active control systems. In order to model these dynamics in the full-band controller, the plant model has been implemented using $J = 512$ coefficient FIR filters at the full sample rate of $Fs = 2.2$ kHz. The full-band control filters have also been implemented with $I = 512$ coefficient FIR filters, as further increases in the control

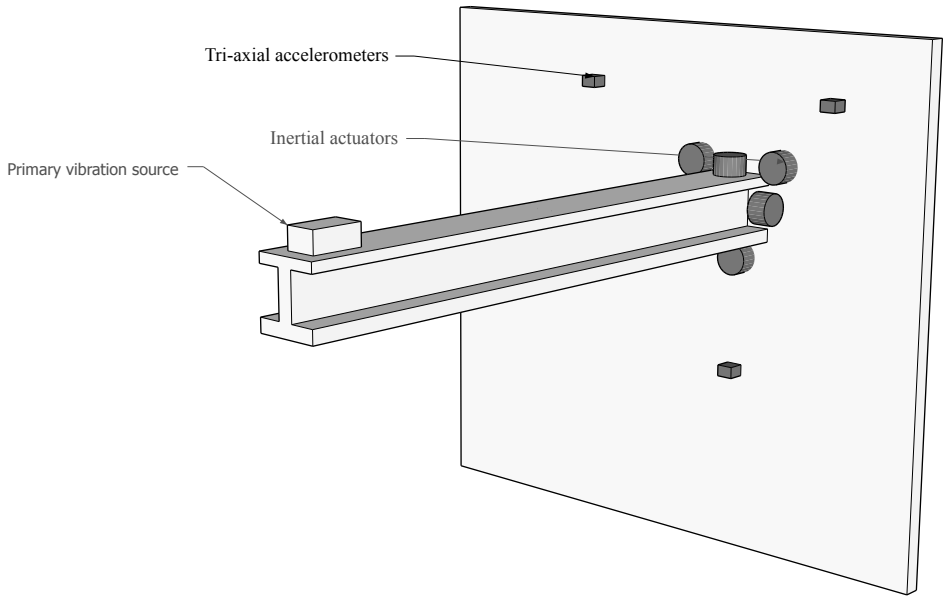

Fig. 5: Test structure representing the transmission of vibration through a beam-like structure into a wall or plate. The control system consists of 5 inertial actuators, shown by the cylindrical objects, and three tri-axial accelerometers, shown by the small cubes on the plate. The primary disturbance is generated by a vibrating source attached to the end of the beam.

filter length did not achieve a significant increase in the level of control.

A. Comparison of the Computational Complexity

Following on from the computational complexity analysis presented in Section III-B, the computational demand required by the different subband implementations and the full-band controller applied to the MIMO control system described above will be investigated. Figure 7 shows the number of multiplications per sample for the individual operations involved in the different multichannel subband active control implementations, as described in Sections III-B1 through to Section III-B5.

Figure 7a shows the number of multiplications required per sample for the generation of the filtered reference signals versus the number of subbands, K. The solid line shows the computational demand given by equation (22) when the plant modelling filters operate on the full-band signals, as shown in Figure 2, and the dashed line shows the computational demand given by equation (24) when the plant modelling filters operate on the subband signals, as shown in Figure 3. It is assumed that the length of the subband plant modelling filters is given by $J_{SAF} = 4J/K$, which is consistent with the subband control filter length reduction. From this plot it can be seen

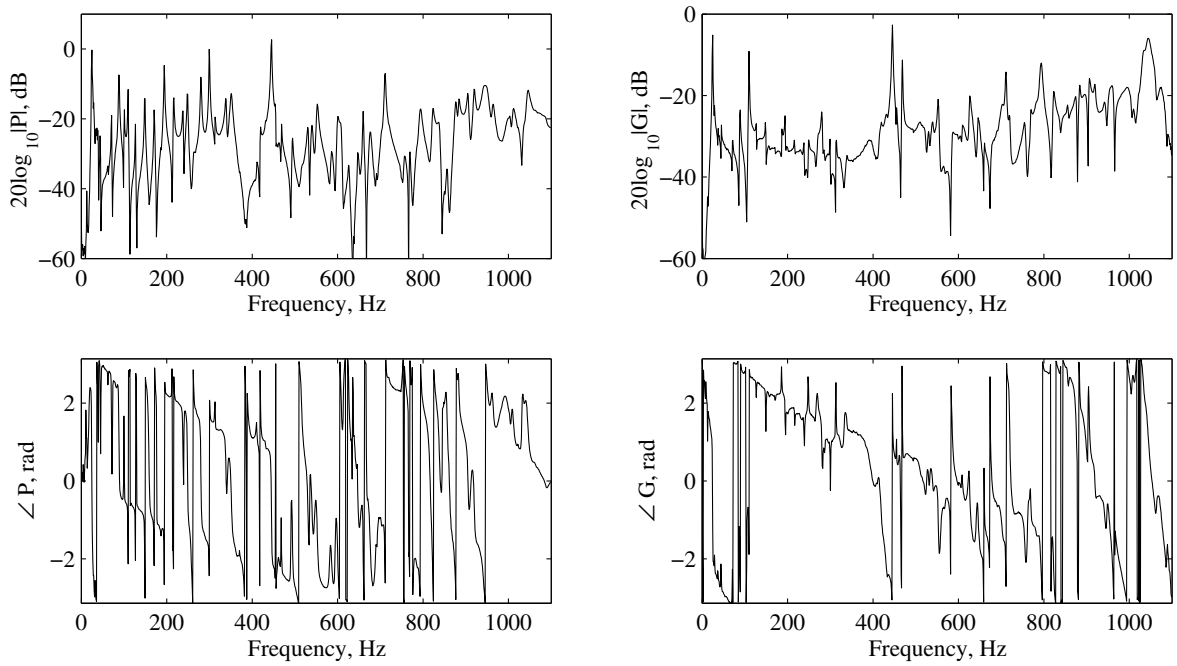

(a) Example primary path response between the primary actuator and error sensor 1.

(b) Example plant response between control actuator 1 and error sensor 1.

Fig. 6: The frequency responses of the primary path (a) and the plant, or secondary path (b).

that the computational demand for the full-band plant modelling implementation is independent of the number of subbands, whereas when the subband plant modelling implementation is employed the computational demand decreases as the number of subbands is increased. The computational demand is higher for the subband plant modelling method when the number of subbands is less than 5, but as the number of subbands employed is increased the computational saving becomes very large. For example, for $K = 1024$ the subband implementation only requires 90 multiplications per sample, whereas the full-band implementation requires 23040 multiplications. These characteristics are consistent with the observations for the SISO case presented in [16].

Figure 7b shows the number of multiplications required per sample for the subband filtering and decimation process versus the number of subbands. The solid lines show the computational demand for the system shown in Figure 2 and the dashed lines show the computational demand for the system shown in Figure 3; the grey lines show the computational demand when the standard analysis filter-bank in Figure 4a is utilised, whereas the black lines show the computational demand when the restructured analysis filter-bank shown in Figure 4b is employed. From this plot it can be seen that the computational demand in all four implementations increases with the number of subbands, which is due to the increase in the number of points required in the inverse FFT. However, it can be seen, by comparing the black and grey lines, that by restructuring the analysis filter-bank using the Noble identity

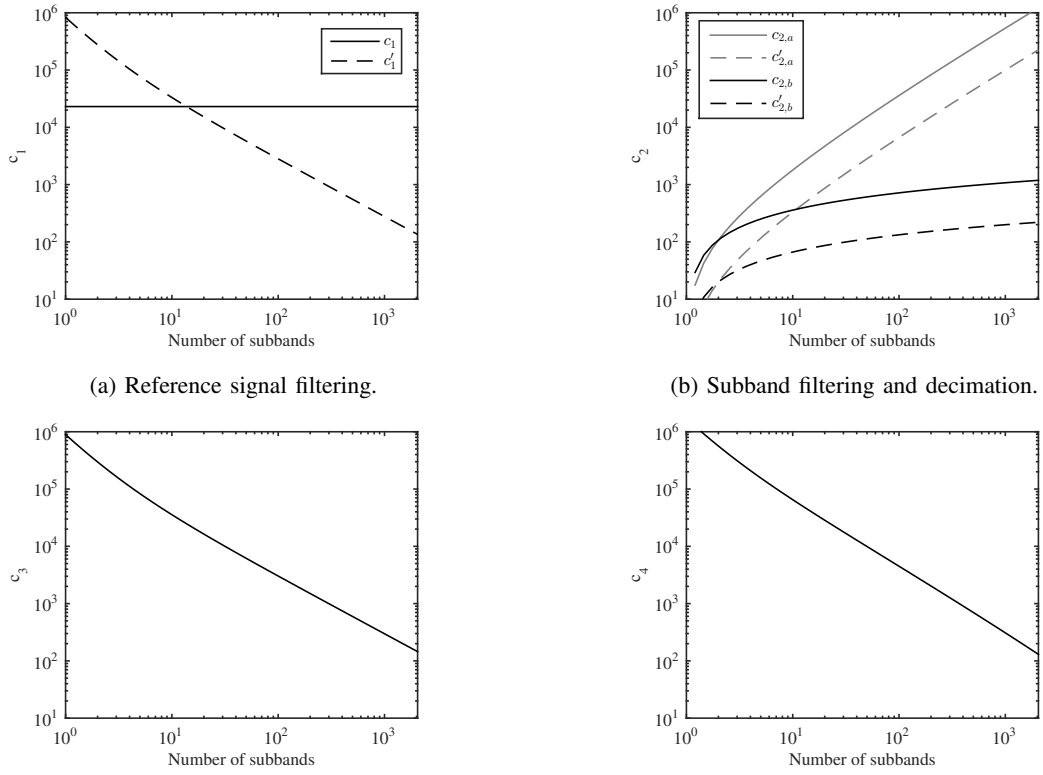

(a) Reference signal filtering.

(b) Subband filtering and decimation.

(c) Subband weight adaptation.

(d) Weight stacking.

Fig. 7: The number of multiplications required per sample for the individual computational operations in the subband control systems implemented according to Fig. 2 (solid lines) and Fig. 3 (dotted lines).

significantly limits the increase in the computational demand that occurs when increasing the number of subbands. It can also be seen from Figure 7b that by employing the subband plant modelling a significant reduction in the computational demand is also achieved, and for the considered system a reduction in the computational demand of 5.4 times the full-band plant modelling implementation is achieved. This computational saving is dependent on the number of control sources, error sensors and reference signals employed in the system. For example, if two reference signals are employed in the MIMO control system the computational reduction is increased to a factor of 9.

The final two subplots in Figure 7 show the number of multiplications required for the subband weight adaptation, c_3, and the weight stacking process, c_4, versus the number of subbands. These two processes are equivalent for the two subband architectures and the number of multiplications per sample are given by equations (31) and (33) respectively. It can be seen that the computational demand for both operations follows a similar trend and decreases as the number of subbands is increased.

The total number of multiplications per input sample for the different implementations of the MIMO filtered-x

LMS active controller with $M = 5$, $L_e = 9$, $L_x = 1$, $I = 512$ and $J = 512$ are shown in Figure 8. The total number of multiplications per sample for the full-band implementation, as detailed in Table I, is due to the generation of the filtered reference signals; the control filter adaptation; and the generation of the control signals. The computational demand for the full-band system is shown in Figure 8 as the dotted line and this provides a comparison for the computational complexity of the subband implementations. The solid lines in Figure 8 show the computational demand for the subband system shown in Figure 2 and the dashed lines show the computational demand for the system shown in Figure 3; the grey lines show the computational demand when the standard analysis filter-bank in Figure 4a is utilised, whereas the black lines show the computational demand when the restructured analysis filter-bank shown in Figure 4b is employed.

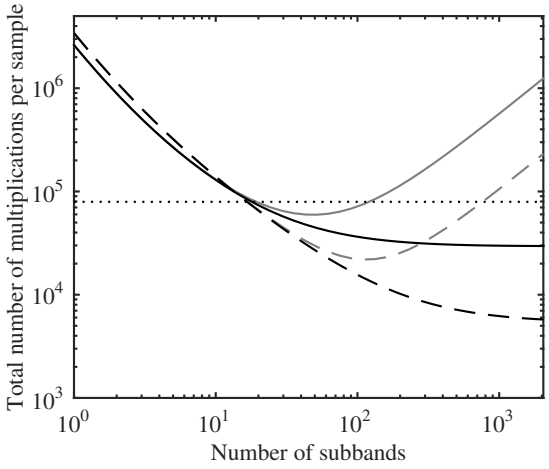

Fig. 8: The number of multiplications required per sample for the MIMO filtered-x LMS active controller implemented using the standard full-band (FB) architecture shown in Fig. 1 (dotted line), the subband (SB) architecture with full-band plant modelling shown in Fig. 2 (solid line), and the subband architecture with subband plant modelling shown in Fig. 3 (dashed line).

From the results in Figure 8 it can be seen that for both subband implementations using the standard analysis filter-bank (Fig. 4a) the computational demand is only lower than the full-band implementation for a relatively narrow range of number of subbands. This range is consistent with the number of subbands employed in both [15], [16] and, therefore, it is possible that this problem was not observed in those investigations. However, it can be seen from the black solid and dashed lines that by employing the restructured analysis filter-bank (Fig. 4b), the computational demand decreases as the number of subbands employed is increased, such that the computational demand is lower than the MIMO full-band algorithm when the number of subbands is greater than around 17 for the system in Figure 2 and 14 for the system in Figure 3. It should be highlighted that these crossover points are dependent on the size of the control system and the length of the control and plant modelling filters, however, the presented results demonstrate the importance of employing the restructured analysis filter-bank, particularly when

a large number of subbands is employed.

It can also be seen from the solid and dashed black lines in Figure 8 that the difference in the computational demand between the two subband implementations increases with the number of subbands. Specifically, it can be seen that the subband implementation with subband plant modelling, as shown in Figure 3, significantly outperforms the subband implementation with full-band plant modelling, as shown in Figure 2. For example, for $K = 1024$ subbands, although the system shown in Figure 2 reduces the number of multiplications compared to the standard full-band controller by a factor of 2.66, the subband implementation shown in Figure 3 reduces the number of multiplications by a factor of 12.88. This highlights the computational benefit of employing the subband implementation shown in Figure 3, however, the performance of the two systems will be compared in the following section.

B. The effect of the number of subbands on performance

It has been shown in Section III-C that the convergence of each of the subband control filters in the MIMO filtered-x LMS algorithm is dependent on the eigenvalue spread of the Hessian matrix in that subband. It has been shown for the SISO subband filtered-x LMS algorithm that the average eigenvalue spread across all subbands reduces as the number of subbands is increased [18], however, it has not been shown directly whether this translates into a consistent increase in the convergence of the error signals and has also not been studied for the MIMO structure. Therefore, for MIMO case, the effect of the number of subbands on both the eigenvalue spread and the convergence speed for the control system outlined above will be investigated.

For the MIMO system considered in this section, the eigenvalue spread of the Hessian matrix, $[\mathbf{R}_k^H(n)\mathbf{R}_k(n)]$, in each subband has been calculated and Figure 9 shows the mean and the standard deviation of the eigenvalue spread across all of the subbands for different numbers of subbands. From these results it can be seen that, as expected, both the mean and standard deviation of the eigenvalue spread decrease as the number of subbands is increased. This result is consistent with the SISO results reported in [18] and according to the convergence analysis presented in Section III-C will result in faster convergence of the subband control filter coefficients.

Although it has been shown that the subband control filter coefficients will converge with time constants that are proportional to the eigenvalue spread of the subband Hessian matrix, and that the average value of the eigenvalue spread reduces as the number of subbands is increased, it is not possible in the case of the subband processing method to then directly infer that this leads to an increase in the convergence of the cost function. This is due to the additional processing on the subband control filter coefficients that is necessary to transform them into the full-band filter coefficients; this is achieved using the weight stacking process described in Section III-A2. This limitation has previously been investigated for a SISO system in [18] and it was shown that the level of attenuation versus the number of subbands generally has a convex upwards relationship, such that the level of control is limited for both small and large numbers of subbands. The convergence of the sum of the squared error signals will therefore be investigated here for the MIMO system.

Figure 10 shows the time taken for the MIMO subband filtered-x LMS algorithm applied to the system shown in

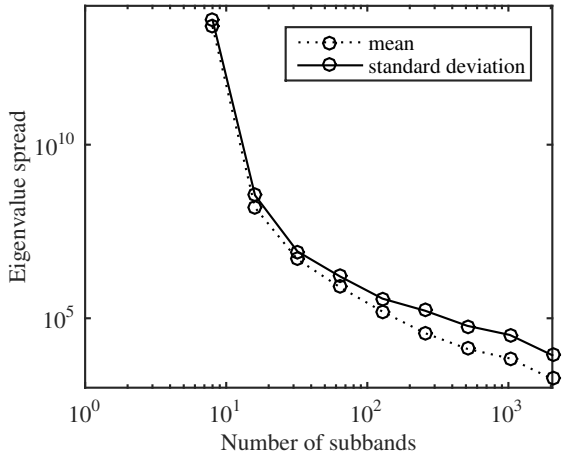

Fig. 9: The mean and standard deviation of the eigenvalue spread of the subband Hessian matrix, $[\mathbf{R}_k^(n)\mathbf{R}_k(n)]$, versus the number of subbands.

Figure 5 to achieve 10 dB of attenuation in the sum of the squared error signals for different numbers of subbands. In each case, the subband convergence gains, α_k, have been set in proportion to the upper limit given by (41), such that the fastest convergence is achieved in each case. From this plot it can be seen that as the number of subbands is increased from the full-band case (i.e. a single subband) the speed of convergence increases, which is consistent with the subband filter weights convergence analysis and the decrease in the eigenvalue spread with an increasing number of subbands. However, it can also be seen from Figure 10 that as the number of subbands increases beyond $K = 512$, the convergence speed reduces. This performance behaviour is consistent with the SISO active noise control systems investigated in [18], [28], where the reduced performance for large numbers of subbands has been linked to the increased distortion due to the weight stacking process.

The frequency response of the ideal weighting stacking process is a brick-wall bandpass filter given by [18]

$$H_k^{ideal}(\omega) = \begin{cases} 1 & |\omega - \frac{2k\pi}{M}| < \frac{\pi}{M} \\ 0 & |\omega - \frac{2k\pi}{M}| > \frac{\pi}{M} \end{cases} . \tag{42}$$

However, in practice, due to the finite length of the DFT used in the weight stacking process, as described in Section III-A2, the response of the weight stacking process will not form a perfect brick-wall filter. The weight stacking will therefore introduce distortion into the system and ultimately limit the control performance. Milani *et al* [28] have proposed a measure of the weight stacking distortion, which is given by the summation over the K subbands of the convolution of the weight stacking response with the ideal response given by (42), and this can be expressed as

$$T(z) = \sum_{k=0}^{K-1} H_k(z) H_k^{ideal}(z). \tag{43}$$

When the response of the weight stacking process is equal to the ideal response, there is no distortion, and

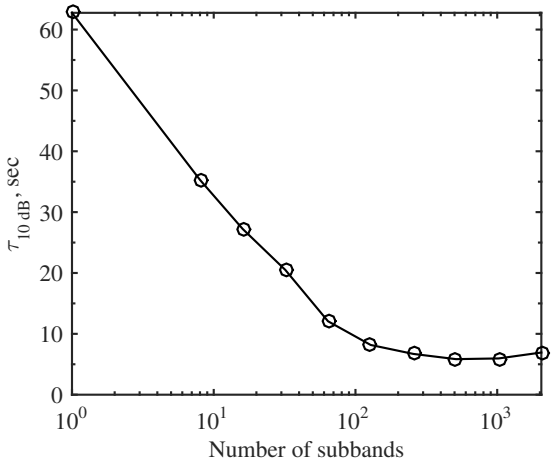

Fig. 10: The time taken for the MIMO subband filtered-x LMS algorithm shown in Figure 2 to achieve 10 dB of attenuation in the cost function versus the number of subbands.

$T(\omega, M) = 1$. The distortion due to the weight stacking process described in Section III-A2 averaged over the full bandwidth is shown in Figure 11 in decibels for a range of numbers of subbands. From this plot it can be seen that the weight stacking distortion increases as the number of subbands increases and indicates why the convergence speed, shown in Figure 10, is limited for large numbers of subbands.

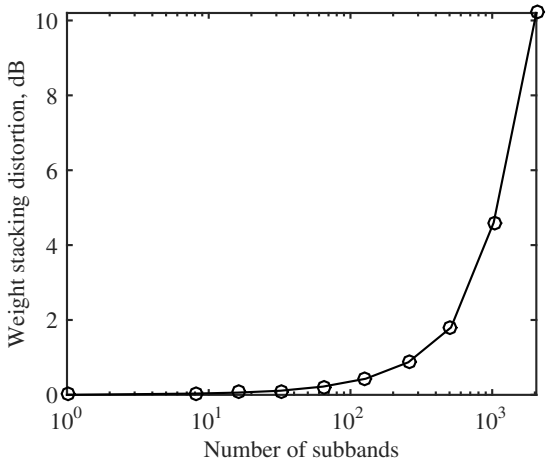

Fig. 11: The weight stacking distortion versus the number of subbands.

C. Direct Comparison of the Two Subband Implementations

From the investigation presented in the previous two sections, it is clear that although the computational demand significantly decreases as the number of subbands is increased, the expected increase in convergence speed only occurs up to a certain number of subbands. That is, although, as expected, the average eigenvalue spread of the Hessian matrix reduces as the number of subbands is increased, the convergence of the cost function is limited by the increase in the weight stacking distortion with the number of subbands. As a result, there is a clear trade-off between the computational demand and the convergence speed. For the practical system considered here, the fastest convergence is achieved with $K = 512$ subbands and, compared to the full-band controller, this corresponds to a 62% reduction in the computational demand for the subband implementation shown in Figure 2 and a 91% reduction for the subband system shown in Figure 3, assuming the subband control filters have a length given by $J_{SAF} = 4J/K$. The performance of the two alternative subband systems using $K = 512$ subbands will, however, be compared in more detail in this section along with the full-band controller.

The performance of the three multichannel algorithms has been assessed for the case when the length of the full-band control filters is $I = 512$, and the subband algorithms have been implemented with $K = 512$ subbands, subband control filters of length $I_{SAF} = 4$, and a decimation factor of $D = 128$. The convergence gain of all three algorithms has been set to give the maximum convergence speed in each case. The convergence gain for each subband, α_k, in the two subband algorithms has been set in proportion to $\frac{2\Re(\lambda_{k_{max}})}{|\lambda_{k_{max}}|^2}$ with the scalar constant of proportionality being set for all subbands such that maximum convergence speed is obtained. The subband convergence gains are presented against frequency in Figure 12, and it is clear from this plot that the subband implementation allows a significant range of convergence gains to be selected over the control bandwidth. The full-band implementation, however, only allows a single convergence gain to be selected and this is limited by the maximum eigenvalue of the full-band Hessian matrix as described by (13).

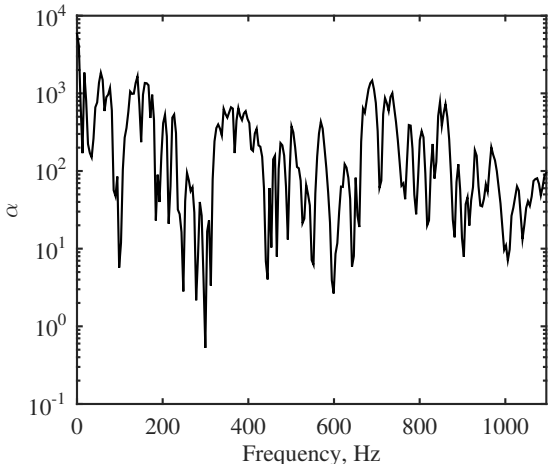

Fig. 12: The subband convergence gains versus frequency.

The spectrum of the cost function, given by the sum of the squared error signals, before control and after the three control algorithms have been adapting for 20 seconds is shown in Figure 13. From this plot it can be seen that the two subband algorithms achieve almost identical broadband attenuation, while the full-band algorithm achieves a lower level of attenuation. The full-band algorithm achieves a broadband average attenuation of 5.6 dB, while the two subband algorithms achieve 12.6 dB of broadband attenuation. The convergence of the cost function for the three algorithms is shown in Figure 14. From this plot it can be seen that the two subband algorithms, as expected, converge significantly faster then the full-band algorithm. The two subband algorithms have almost identical convergence behaviour, with the small variation being attributed to small differences between the outputs of the full-band and subband plant models used in the two algorithms due to the influence of the out-of-band subband plant modelling error and the fact that the subband filtering does not provide perfect brick-wall filtering. Nevertheless, it is clear that the multichannel subband algorithms are capable of achieving a significant increase in the convergence speed compared to the full-band algorithm, whilst also achieving significant reductions in the computational demand.

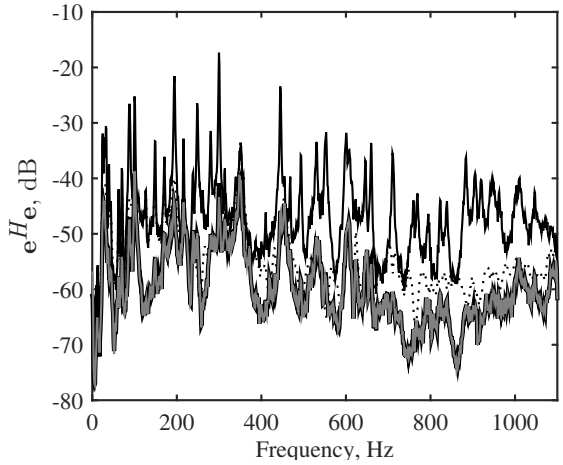

Fig. 13: The spectrum of the cost function, given by the sum of the squared error signals, before control (thin solid black line) and after 20 seconds of convergence using the full-band algorithm (thin dotted black line), the subband algorithm with full-band plant modelling (thick solid black line) and the subband algorithm with subband plant modelling (thin solid grey line).

V. Conclusions

The performance and practical applications of broadband multichannel active noise and vibration control systems are limited by both the large computational demand and the slow convergence speed. These limitations have been addressed in the case of SISO control systems using subband adaptive algorithms, and this paper has presented a thorough investigation of the extension of these algorithms to multichannel active control systems. In particular,

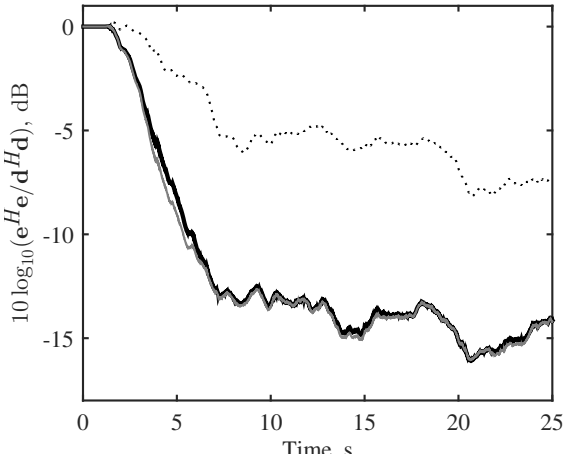

Fig. 14: The convergence envelope of the cost function, given by the sum of the squared error signals, for the full-band algorithm (thin dotted black line), the subband algorithm with full-band plant modelling (thick solid black line) and the subband algorithm with subband plant modelling (thin solid grey line)

two successful SISO subband adaptive algorithms have been extended to the MIMO application. The first of these MIMO subband filtered-x LMS algorithms implements the plant model using a bank of full-band FIR filters, whilst the second implementation, proposed by Park *et al* [16], decomposes the plant response into subband models which are implemented at the decimated sample rate.

The computational complexity of these two MIMO implementations has firstly been compared to the standard full-band MIMO controller and it has been shown that in both cases the computational saving increases as the number of subbands employed is increased. However, this is only the case if the Noble identity is utilised to restructure the subband analysis filter bank and decimation process, which has not previously been highlighted. Additionally, the computational saving achieved in the multichannel case by the subband algorithm with subband plant modelling is significantly greater than the standard subband algorithm with full-band plant modelling, which was originally proposed by Morgan and Thi [15].

In addition to the computational saving, it has been suggested in the literature that the MIMO subband active noise control algorithm could provide an increase in the convergence speed, however, no analysis of the convergence behaviour or investigation into the practical improvements has been presented. Therefore, an analysis of the convergence of the MIMO subband control filter coefficients has been presented and it has been shown that the convergence in each subband is dependent on the spread of the eigenvalues of the subband Hessian matrix. It has then been shown for a practical, MIMO active vibration control system that the mean and standard deviation of the subband eigenvalue spread decreases as the number of subbands is increased. However, it has then been shown that this does not in fact translate into an increase in the convergence speed as the number of subbands is increased. It has been shown that this is due to the increase in the distortion introduced by the weight stacking process as

the number of subbands is increased. As a result, there is a trade-off between the computational demand and the control performance.

Finally, the overall performance of the practical active vibration control system has been assessed for the two subband algorithm implementations and the standard full-band algorithm. In this case the subband algorithms have both been implemented using the $K = 512$ subbands, which gives the fastest convergence speed for the considered system. It has then been shown that the two subband implementations significantly outperform the standard full-band implementation in terms of the speed of convergence and, therefore, the level of control after a fixed period of convergence time. Importantly, it has also been shown that the MIMO subband algorithm employing a subband plant model achieves identical performance to the less computationally efficient algorithm that employs a fullband plant model.

REFERENCES

[1] S. J. Elliott, *Signal Processing for Active Control*. London: Academic Press, 2001.

[2] C. Hansen, S. Snyder, X. Qiu, L. Brooks, and D. Moreau, *Active control of noise and vibration*. CRC Press, 2012.

[3] S. M. Kuo and D. Morgan, *Active noise control systems: algorithms and DSP implementations*. John Wiley & Sons, Inc., 1995.

[4] E. A. Wan, "Adjoint lms: An efficient alternative to the filtered-x lms and multiple error lms algorithms," in *Acoustics, Speech, and Signal Processing, 1996. ICASSP-96. Conference Proceedings., 1996 IEEE International Conference on*, vol. 3, pp. 1842–1845, IEEE, 1996.

[5] S. C. Douglas, "Fast implementations of the filtered-x lms and lms algorithms for multichannel active noise control," *IEEE Transactions on speech and audio processing*, vol. 7, no. 4, pp. 454–465, 1999.

[6] S. M. Kuo and D. R. Morgan, "Active noise control: A tutorial review," *Proceedings of the IEEE*, vol. 87, pp. 943–973, June 1999.

[7] Y. Wang, C. Zhang, and Z. Wang, "A new variable step size lms algorithm with application to active noise control," in *Acoustics, Speech, and Signal Processing, 2003. Proceedings.(ICASSP'03). 2003 IEEE International Conference on*, vol. 5, pp. V–573, IEEE, 2003.

[8] L. Wu, X. Qiu, I. S. Burnett, and Y. Guo, "A recursive least square algorithm for active control of mixed noise," *Journal of Sound and Vibration*, vol. 339, pp. 1–10, 2015.

[9] R. M. Reddy, I. M. Panahi, and R. Briggs, "Hybrid fxrls-fxnlms adaptive algorithm for active noise control in fmri application," *IEEE Transactions on Control Systems Technology*, vol. 19, no. 2, pp. 474–480, 2011.

[10] M. Ferrer, A. Gonzalez, M. de Diego, and G. Pinero, "Fast affine projection algorithms for filtered-x multichannel active noise control," *IEEE transactions on audio, speech, and language processing*, vol. 16, no. 8, pp. 1396–1408, 2008.

[11] J. Lorente, M. Ferrer, M. De Diego, and A. González, "Gpu implementation of multichannel adaptive algorithms for local active noise control," *IEEE/ACM Transactions on Audio, Speech, and Language Processing*, vol. 22, no. 11, pp. 1624–1635, 2014.

[12] B. Rafaely and S. J. Elliott, "Rapid frequency-domain adaptation of causal fir filters," *IEEE Signal Processing Letters*, vol. 4, no. 12, pp. 337–339, 1997.

[13] B. Rafaely and S. J. Elliott, "A computationally efficient frequency-domain lms algorithm with constraints on the adaptive filter," *IEEE Transactions on Signal Processing*, vol. 48, no. 6, pp. 1649–1655, 2000.

[14] N. K. Rout, D. P. Das, and G. Panda, "Computationally efficient algorithm for high sampling-frequency operation of active noise control," *Mechanical Systems and Signal Processing*, vol. 56–57, pp. 302 – 319, 2015.

[15] D. Morgan and J. Thi, "A delayless subband adaptive filter architecture," *IEEE Transactions on Signal Processing*, vol. 43, pp. 1819–1830, August 1995.

[16] S. Park, J. H. Yun, Y. Park, and D. Youn, "A delayless subband active noise control system for wideband noise control," *IEEE Transactions on Speech and Audio Processing*, vol. 9, pp. 892–899, November 2001.

[17] A. Milani, I. Panahi, and P. Loizou, "A new delayless subband adpative filtering algotithm for active noise control systems," *IEEE Transactions on Audio, Speech, and Language Processing*, vol. 17, pp. 1038–1045, July 2009.

[18] A. Milani, G. Kannan, I. Panahi, and R. Briggs, "Analysis and optimal design of delayless subband active noise control systems for broadband noise," *Signal Processing*, vol. 90, pp. 1153–1164, 2010.

[19] S. Weiss, R. G. W., and R. W. Steward, "Multichannel equalization in subbands," in *Proc. IEEE Workshop on Applications of Signal Processing to Audio and Acoustics*, (New Paltz, New York), Oct. 1999.

[20] X. Qiu, N. Li, G. Chen, and C. Hansen, "The implementation of delayless subband active noise control algorithms," in *Proceedings of Active*, vol. 6, (Adelaide, Australia), pp. 18–20, September 2006.

[21] S. J. Elliott, I. M. Stothers, and P. A. Nelson, "A multiple error LMS algorithm and its application to the active control of sound and vibration," *IEEE Transactions on Acoustics, Speech, and Signal Processing*, vol. 35, pp. 1423–1434, October 1987.

[22] S. Elliott and P. Nelson, "Active noise control," *IEEE Signal Processing Magazine*, vol. 10, pp. 12–35, Oct 1993.

[23] B. Widrow and S. Sterns, *Adaptive signal processing*. Englewood-Cliffs, NJ: Prentice-Hall, 1985.

[24] P. P. Vaidyanathan, *Multirate systems and filter banks*. Prentice Hall, 1993.

[25] K.-A. Lee, W.-S. Gan, and S. Kuo, *Subband adaptive filtering: theory and implementation*. John Wiley & sons, 2009.

[26] N. Hirayhama, H. Sakai, and S. Miyagi, "Delayless subband adaptive filtering using the hadamard transform," *IEEE Transactions on Signal Processing*, vol. 47, pp. 1731–1734, June 1999.

[27] R. Merched, P. Diniz, and M. Petraglia, "A new delayless subband adpative filter structure," *IEEE Transactions on Signal Processing*, vol. 47, pp. 1580–1591, August 2002.

[28] A. Milani, G. Kannan, I. Panahi, and R. Briggs, "Weight stacking analysis in delayless subband adaptive algorithm for fMRI active noise control," in *IEEE Engineering in Medicine and Biology Workshop*, 2007.

Jordan Cheer Jordan Cheer received the B.Mus. (Tonmeister) degree in music and sound recording from the Institute of Sound Recording, University of Surrey, U.K. in 2008, and the M.Sc. and Ph.D. degrees in sound and vibration studies from the Institute of Sound and Vibration Research (ISVR), University of Southampton, U.K., in 2009 and 2012, respectively.

From 2012 to 2014, he was a Research Fellow in Active Control at the ISVR. He was promoted to a Senior Research Fellow in 2015 and currently holds a New Frontiers Fellowship at the same institution. His research has focused on the active control of noise and vibration and array signal processing for audio reproduction. He has published 45 papers in journals and conference proceedings and is an Assistant Editor for the Journal of Sound and Vibration.

Dr. Cheer is a Member of the International Institute of Acoustics and Vibration and a Fellow of the Higher Education Academy. He received the P. E. Doak Award for academic performance in the taught part of the M.Sc., the E. J. Richards Prize for the best masters dissertation, and the Sir James Lighthill Award for the best student paper at the 19th International Congress on Sound and Vibration. He also served on the scientific committees for the 24th International Congress on Sound and Vibration and the 2016 Audio Engineering Society Conference on Sound Field Control.

Steve Daley Steve Daley received the B.Sc. degree in mechanical engineering and the Ph.D degree from the University of Leeds, U.K. in 1981 and 1984 respectively.

From 1984 to 1986, he was working as a researcher at the GEC Engineering Research Centre (ERC). In 1986 he joined the Department of Electrical Engineering and Electronics at Brunel University as a Lecturer in Control Engineering. In 1990 he rejoined ERC and following the acquisition of the Centre by ALSTOM in 1996 was promoted to Technology Head for Control and Monitoring. In 2003 he returned to an academic position as Professor of Industrial Control in the Department of Automatic Control and Systems Engineering at the University of Sheffield and moved to the ISVR in 2010 where he is currently the Head of the Signal Processing and Control Group. He has published widely on a broad variety of applications focussed control systems research. He serves on the editorial boards of the Proceedings of the Institution of Mechanical Engineers, Part I and Control Engineering Practice.

Prof. Daley is a Chartered Engineer and a Fellow of the Institution of Mechanical Engineers. He has been the recipient of numerous prizes and awards for his work including the 1999 Honeywell International Medal from the Institution of Measurement of Control and the 1988 Thomas Bernard Hall Prize from the Institution of Mechanical Engineers.